Activation of Ultra-Thin Activated Carbon Fibers as Electrodes for High Performance Electrochemical Double Layer Capacitors

Yen-Ju Su,[1] Tes-Hao Ko,[1] Shu-Hui Cheng,[2] Wan-Shu Chen,[2] Tzu-Hsien Han,[2] Jui-Hsiang Lin[1]

[1]*Department of Material Science and Engineering, Feng Chia University, Taichung 40724, Taiwan*
[2]*Material and Chemical Research Laboratories, Industrial Technology Research Institute, Hsinchu 30071, Taiwan*

Received 3 April 2008; accepted 14 August 2008
DOI 10.1002/app.29092
Published online 30 October 2008 in Wiley InterScience (www.interscience.wiley.com).

ABSTRACT: Activated carbon fibers (ACFs) contain pores with a weak resistance to electrolyte migration but with high electrical resistance between the fibers. The ACFs used herein were prepared from ultra-thin polyacrylonitrile (PAN) fibers, to be used as electrodes in electrochemical double layer capacitors (EDLCs), by varying the activation temperatures and the holding times during steam activation. As the activation temperature and holding time were increased, the specific surface area increased along with the specific capacitance (F g^{-1}). A maximum specific capacitance as high as 283 F g^{-1} can be obtained using the ultra-thin ACFs fabricated at 1000°C for 10 min with a specific surface area of 1408 m^2 g^{-1}. This investigation demonstrates that the surface area, pore structure, and surface functional groups of ACFs were all significant factors in determining the capacitive characteristics of ACFs. © 2008 Wiley Periodicals, Inc. J Appl Polym Sci 111: 1615–1623, 2009

Key words: fibers; electrochemical double layer capacitors; steam activation; specific surface area; PORE structure

INTRODUCTION

Porous carbon materials, collectively called activated carbons (ACs), are generally prepared by activation using either physical or chemical methods.[1–3] Developing novel adsorbents with fibrous morphology like that of activated carbon fibers (ACFs) is attracting increasing interest. The properties, including specific surface area, pore volume, and porosity, of ACFs were found to be strong functions of the activation procedure and the species of the raw materials.[4] Polyacrylonitrile (PAN),[5] coal and petroleum-based pitches,[6] cellulose[7] and phenolic resin[8] have been selected as raw materials in fabricating precursor fibers. The benefits of ACFs are their smaller fiber diameter than with those for conventional activated granular/powder carbons (which minimizes diffusion limitations and allows rapid adsorption/desorption), more concentrated pore size distribution, and excellent adsorption capacity at low concentrations of adsorbates. Typically, an ACF is a carbonaceous adsorbent with slit-shaped micropores, which are the source of the high adsorption capacity that makes ACFs effective adsorbents, catalysts, and catalyst supports.

In 1879, Helmholtz suggested that electrochemical double layer capacitors (EDLCs) accumulate electrical energy that is generated by the formation of an electrochemical double layer suggested, at the interface between electrode and electrolyte (non-Faradaic process), unlike secondary batteries such as the lithium ion battery or nickel metal hydride battery, which are based on a redox reaction (Faradaic process). This energy storage system based on a non-Faradaic process provides very fast charge and discharge making the EDLCs with the best candidates to meet the demand for high power and long durability. Recently, the relationships between the porous structures and electrochemical behavior have become increasingly important.[9] Although the use of various materials as EDLCs has been investigated, the application is limited in terms of specific energy. To enhance the specific energy and power of EDLCs, several researchers have put much effort into the development and modification of carbonaceous materials, such as controlling the pore size distribution, introducing electro-active metallic particles or electro-conducting polymers, and fabricating hybrid-type cells.[10,11] The porosity of the ACFs is a key factor in determining the capacitive performance of EDLCs because a complete array of the electric double layers can be established and solvated ions can move freely within such pores.[12] ACFs that are manufactured under various conditions have different

Correspondence to: Y.-J. Su (keigosuru@yahoo.com.tw).
Contract grant sponsors: Biomedical and Technical Fibers Department of Industrial Technology Research Institute, Republic of China.

pore structures and surface conditions typically resulting in the incomplete utilization of the surface area (i.e., electrochemically inaccessible/partially accessible).[13] Additionally, the capacitance per unit area (in F cm^{-2}) varies among the accessible surface areas because of the presence of various functional groups.[14] Therefore, numerous works have been performed to modify the surface properties of ACFs and thus optimize their capacitive performance (i.e., high power and high specific capacitance).[9,12–14]

The aim of this investigation is to prepare various ACFs by varying the activation temperature and the holding time and then to evaluate their effectiveness in EDLCs. Furthermore, the physical properties such as BET surface area, pore size distribution, total pore volume, surface functional groups, and yield of steam ACFs are systematically characterized. Finally, an attempt is made to elucidate a correlation between the adsorption behavior of particular species and the capacitive performance of the EDLCs upon charge/discharge.

EXPERIMENTAL

Treatments and preparation of materials

Ultra-thin polyacrylontrile (PAN) fiber felts having average diameters around 4.75 μm, supplied by Industrial Technology Research Institute, were used as precursors to yield ACFs. Stabilization was attained in a constant temperature zone furnace at 280°C for 15 min in air atmosphere with a heating rate of 2°C min^{-1}. Stabilized fibers were activated by passing them through a ceramic reaction tube. During activation, stabilized fibers were heat treated in H_2O at 900 and 1000°C for 5, 10, and 15 min. After activation, the ACFs were used as electrode material of EDLCs.

Characterization and measurements

Micromeritics ASAP 2020 accelerated surface area and porosimetery apparatus (Micrometics Ins. Corp.) was used for volumetric measurement nitrogen adsorption isotherms at 77 K and relative pressure from 10^{-6} to 1. High-purity (99.999%) nitrogen was used; before measurement all samples were degassed at 300°C for 6 h. Nitrogen adsorption experiments were performed in static mode using mass flow controller programmed to supply fixed dose of nitrogen to sample container. After equilibration, pressure was recorded and process contained at higher dose pressures until saturation pressure was reached. Difference between previous and next equilibrated pressure, along with dose volume, was used to calculate the amount of nitrogen adsorbed by sample. The specific surface area was calculated from the isotherms by using the Brunauer-Emmett-Teller (BET) equation.[15] The pore size distributions (PSDs) appear to be especially useful information about porous carbons. Nitrogen adsorption is a standard procedure for the determination of PSDs. The density functional theory (DFT) program performs an inversion of the integral equation for the overall adsorption with respect to the PSDs. The experimental adsorption isotherm measured on a sample of a porous solid is the aggregate of the isotherm for the individual pores that make up the pore structure of the solid. In mathematical terms, the experimental isotherm is the integral of the single pore isotherm multiplied by the pore size distribution. For a slit-shaped pore, this can be written as[16–19]:

$$N(p) = \int_{H_{\min}}^{H_{\max}} f(H)\rho(p,H)dH$$

where $N(p)$ is the number of moles adsorbed at a pressure p, $H_{\min}$ and $H_{\max}$ are the widths of the smallest and largest pores present (where the pore width is the distance between the nuclei of carbon atoms on opposing pore walls), respectively, and [*1/2*](p; H) is the molar density of nitrogen at pressure p in a pore of width H. The pore size distribution, $f(H)$, is the distribution of pore volumes as a function of pore width. In this approach, the individual model isotherm [*1/2*](p; H) comes from the molecular model of nitrogen adsorption on the basis of nonlocal or smoothed density approximation. To ensure numerical stability of the inversion of the integral equation, the regularization method is employed. DFT was first used as the basis of a practical method for determining PSD in the range from micropore to mesopore by Seaton et al.[18] These workers assumed that the PSD of a sample could be described by a bimodel lognormal distribution function; the six parameters of the distribution were determined by a multilinear least square fitting of parameterized computed model isotherm to the data. Oliver[19] extended and generalized the method by numerical deconvolution of the distribution result from micropore to macropore.

Supercapacitor cells with three electrodes were built by assembling 1 cm^2 ACFs-felt electrodes with polypropylene separator. An Ag/AgCl (saturated KCl) electrode and a Pt electrode were used as the reference and counter electrode, respectively. The electrode performances were measured in 1*M* H_2SO_4 at 25°C. The charge–discharge curves were galvanostatically measured with a CHI 608C electrochemical working station (CH Instruments, USA) in the potential range of 0–0.75 V and at a constant current

TABLE I
Parameters Characterizing the Porous Structure of ACFs

Activation temperature (°C)	Hold time (min)	Yield (wt %)	S_{BET}[a] ($m^2\ g^{-1}$)	$V_{0.95}$[b] ($cm^3\ g^{-1}$)	MPD[c] (Å)	*t*-plot ($m^2\ g^{-1}$) Micropore area	*t*-plot ($m^2\ g^{-1}$) External Surface area
900	5	62.9	767	0.1929	9.3747	679	87
	10	60.6	962	0.2142	9.4448	789	173
	15	57.8	1294	0.2352	9.5111	970	324
1000	5	49.8	854	0.2042	9.4342	694	160
	10	47.9	1408	0.2459	9.5389	965	444
	15	44.8	1081	0.2215	9.5696	729	353

[a] S_{BET}, BET surface area.
[b] $V_{0.95}$, total pore volume estimate at relative pressure 0.95.
[c] MPD, median pore width.

of 1 mA. The cell capacitance was calculated from the slope of the discharge:

$$C = \frac{(I \times \Delta T)}{\Delta V}$$

where C is the capacitance of the cell in farads; I is the discharge current in amperes; ΔT is the discharging time from 0.7 to 0.05 V; and ΔV is the potential variation in the time range measured, i.e., the slope in volts per second ($V\ s^{-1}$). In a symmetrical system, the specific capacitance C_m in farads per gram of samples ($F\ g^{-1}$) is related to the capacitance of the cell C:

$$C_m = \frac{C}{m}$$

where m is the weight (g) per electrode.

Cyclic voltammetry of the unit cell was performed in the potential range of 0–0.75V with scan rates 6 $mV\ s^{-1}$.

A photoelectron spectrometer ESCA LAB 250R (VG Scientific Co., UK) with a monochromatic Al K_α X-ray source (1486.6 eV) was used, and the samples were fixed on an indium support. The area analyzed consisted of a circular region of 1 mm^2, and the kinetic energy of the heart electrons coming from the first atomic layers of the solids is measured through hemispherical analyzers. The results were expressed as spectra of counts at the detector versus binding energy, and the surface atomic concentrations were calculated.

The micro-Raman spectra (Renishaw Raman imaging microscope system 2000) were acquired by using a He-Ne laser of 25 mW and 632.9 nm as excitation wavelength. The microbeam of about 2 mm diameter was moved fast in a random pattern over the samples to avoid local heating by the laser light. The scattered radiation was collected in a region between 800 and 2000 cm^{-1}. The graphitic (G, 1580 cm^{-1}) and defect (D, 1350 cm^{-1}) peaks were measured. The I_G/I_D ratio was calculated by fitting the peaks using a mixed Gaussian-Lorentzian curve fitting procedure.[20] A total of five scans were collected and averaged for each sample.

RESULTS AND DISCUSSION

The pore properties of the ultra-thin activated carbon fibers

Table I summarizes the yield of the final products and the Brunauer-Emmett-Teller (BET) surface area in the fabrication of ACFs from ultra-thin PAN fibers. The products were obtained by heating to 900 and 1000°C for 5, 10, and 15 min.

As is well known, activation with steam as a gasifying agent involves C-H_2O reactions, removing carbon atoms and causing most of the weight loss of the resulting ACFs. At all activation temperatures from 900 to 1000°C, as the holding time was increased from 5 to 15 min, the yield of the ultra-thin ACFs decreased continuously because of release of volatile matter and the burn-off reaction between carbon and the steam atmosphere. At a higher temperature of 1000°C, as the holding time was increased from 5 to 15 min, the decrease in yield exceeded at 900°C. A severe reaction during activation, which results in the development of internal surface areas and porosities, explains why the burn-off of carbon at this excessively high temperature was responsible for most of the decrease in yield.

Table I presents the characteristics of the resulting ACFs determined by N_2 gas adsorption at 77 K. When the activation temperature was maintained at 900°C, increasing the holding time to 15 min increased the BET surface area. The increase in the BET surface area and median pore width (MPD) with the increase of activation time was also evident at an activation temperature of 1000°C. The optimal activation condition for the ultra-thin ACFs was 1000°C for 10 min, which yielded the highest BET surface area (1408 $m^2\ g^{-1}$) and total pore volume

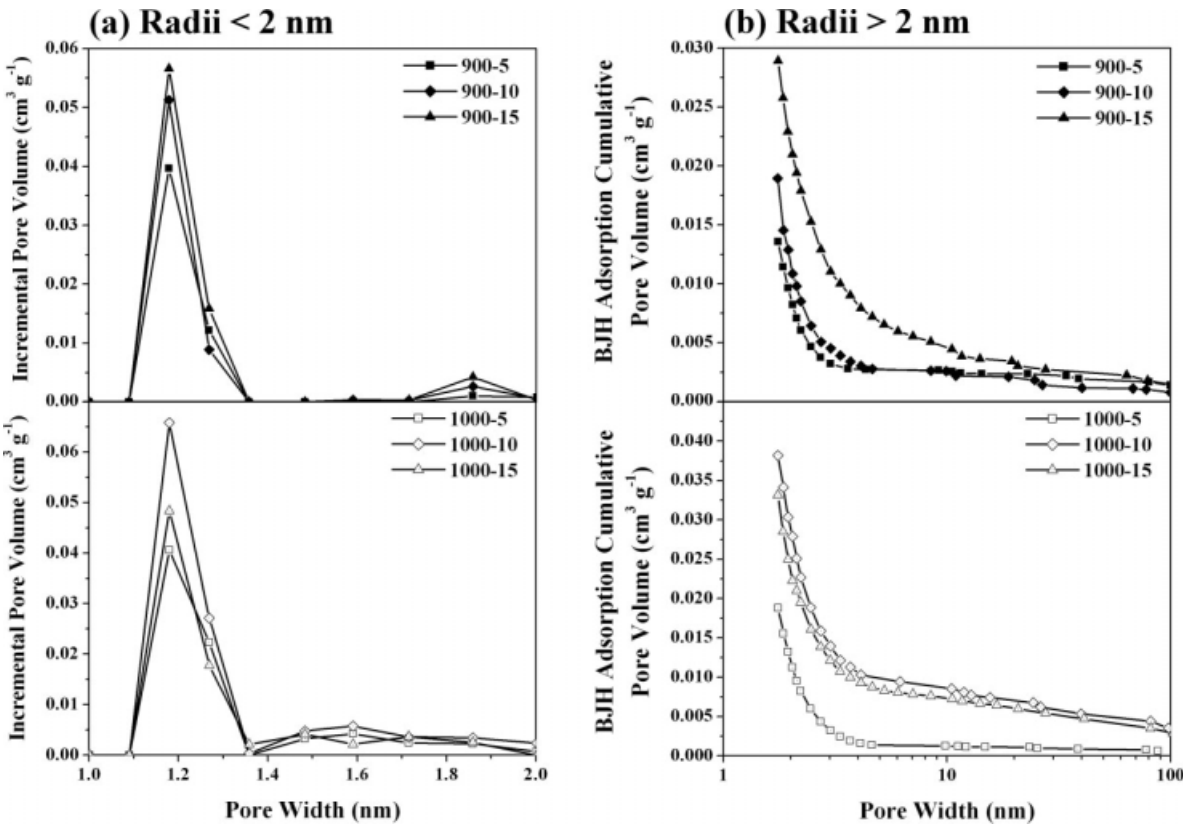

Figure 1 Pore size distributions of ultra-thin ACFs prepared at different activation temperatures and various holding times: (a) evolution of micropore and (b) evolution of mesopore/macropore.

(0.2459 cm^3 g^{-1}). However, in the case of steam activation at 1000°C for 15 min, the BET surface area and the total pore volume decreased because of the severe reaction of C-H_2O and the increase in burn-off, resulting in the conversion of microporosities into mesoporosities or even macroporosities. Because the destruction of high porosity by external ablation of carbon particles exceeds the development and widening of micropores, the BET surface area and the total pore volume are reduced at 15 min, but the pore width is increased.

According to the classification that was adopted by the International Union of Pure and Applied Chemistry (IUPAC), pores are classified as micropores (<2 nm diameter), mesopores (2–50 nm diameter), or macropores (>50 nm diameter).[21] Pore size distribution (PSD) was adopted to analyze the full range of pore sizes in ultra-thin ACFs, the micropores obtained by density functional theory (DFT), and the mesopores/macropores obtained by the BJH method. The average pore size distribution depends mainly on the temperature and holding time of activation. The micropores in ultra-thin ACFs were responsible for most of the pore volume, whereas mesopores and macropores contribute less pore volume (Fig. 1). This result indicates that ACFs with bimodal pore structures had been obtained with pores of diameter < 2 nm and pores of diameter > 2 nm. As the activation temperature is increased from 900 to 1000°C and the holding time is increased from 5 to 15 min, more pores were formed, significantly, increasing the pore volume. A total pore volume of 0.1929 cm^3 g^{-1} was obtained at an activation temperature of 900°C for 5 min, increasing with holding time to 0.2352 cm^3 g^{-1} (900°C, 15 min) and with activation temperature to 0.2042 cm^3 g^{-1} (1000°C, 5 min). Figure 1 demonstrates that the distribution patterns of pores of all ACFs are similar. Two peaks are obtained at each activation temperature, centered at 1.18 and 1.86 nm at 900°C and at 1.18 and 1.59 nm at 1000°C; a sharp increase in pore volume revealed the formation of micropores [Fig. 1(a)]. This increase in the volume of pores in mesopores became markedly significant in the ultra-thin ACFs, which were prepared at 1000°C for 5 to 10 min [Fig. 1(b)]. As the activation temperature and holding time were further increased, the pore volume also increased, because new pores (mainly micropores) were formed, and all pores were widened, as revealed by the total pore volume and the DFT results. However, ultra-thin ACFs that were prepared at 1000°C for 15 min had lower pore volumes both of micropores and of mesopores/macropores than the ACFs that were prepared at 1000°C

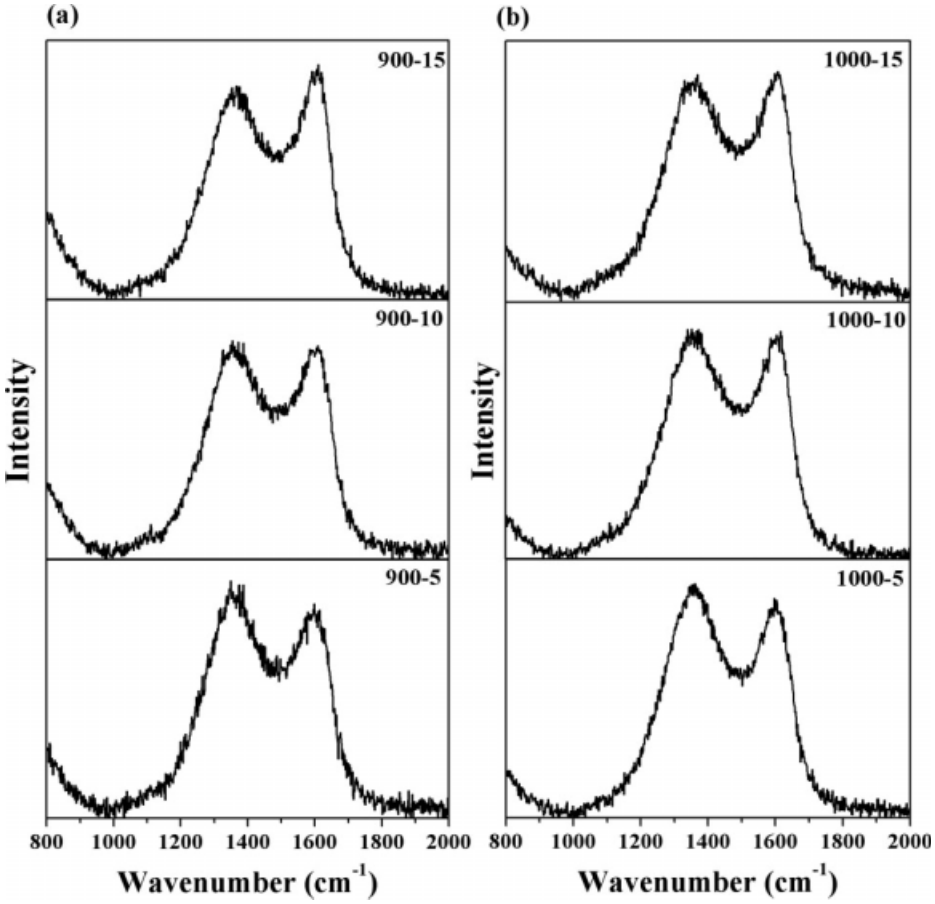

Figure 2 Raman spectra of ultra-thin ACFs prepared at (a) 900°C and (b) 1000°C.

for 10 min. The severe reaction of C-H_2O and the release of volatile matter, which widen pores and cause the combination of micropores, reduced the pore volume in ACFs that were prepared from 15 min. Therefore, the optimal activation conditions were verified to be an activation temperature of 1000°C and a holding time of 10 min. The surface areas and porosities in ultra-thin ACFs developed under these conditions were supposed to be the most suitable for applications in electrodes of electrochemical double layers capacitors (EDLCs).

Figure 2 presents the effect of activation temperatures and holding times on the Raman spectra of the ultra-thin ACFs. The Raman profile was fitted to the G (1580) and D (1360) bands which have already been identified in various types of carbon. The G line is obtained at 1580 cm^{-1} in single crystal graphite; the D line is at 1360 cm^{-1} and is thought to be associated with structural imperfections.[11] The Raman cross section for sp^2-bonded C significantly exceeds that of sp^3-bonded C in the visible region. Therefore, the Raman spectra only reveal the state of the sp^2-bonded C in the sp^3 matrix. Tuinstra and Koening[12] related the intensity ratio between D- and G-band (I_D/I_G intensity ratio) to the XRD dimensions of graphite nanoparticles (L_a) along the basal plane, according to the equation

$$\frac{I_D}{I_G} = \frac{44}{L_a}$$

The L_a-value of ACFs activated at 900°C was 1.76 to 2.29 nm upon activation from 5 to 15 min. However, the L_a-value of ACFs activated at 1000°C increased with the holding time up to 2.74 nm (10 min) and decreased upon further activation, revealing that the severe reaction introduced defects into the ultra-thin ACFs during activation.

Figures 3 and 4 present the spectra of ESCA and C 1s. The main peaks of carbon (C 1s), oxygen (O 1s), and nitrogen (N 1s) between binding energies 200 and 600 eV correspond to graphite-like carbon and various functional groups. The C 1s peak at 284.6 eV was associated with the carbon element only; that between 284.05 and 284.83 eV was associated with graphitic carbon; 285.08 and 285.42 eV was associated with hydroxyl (>C—OH); 287.34 and 288.49 eV was associated with carbonyl (>C=O) and that between 290.13 and 290.92 eV was associated with carboxylic (—COOH) functional

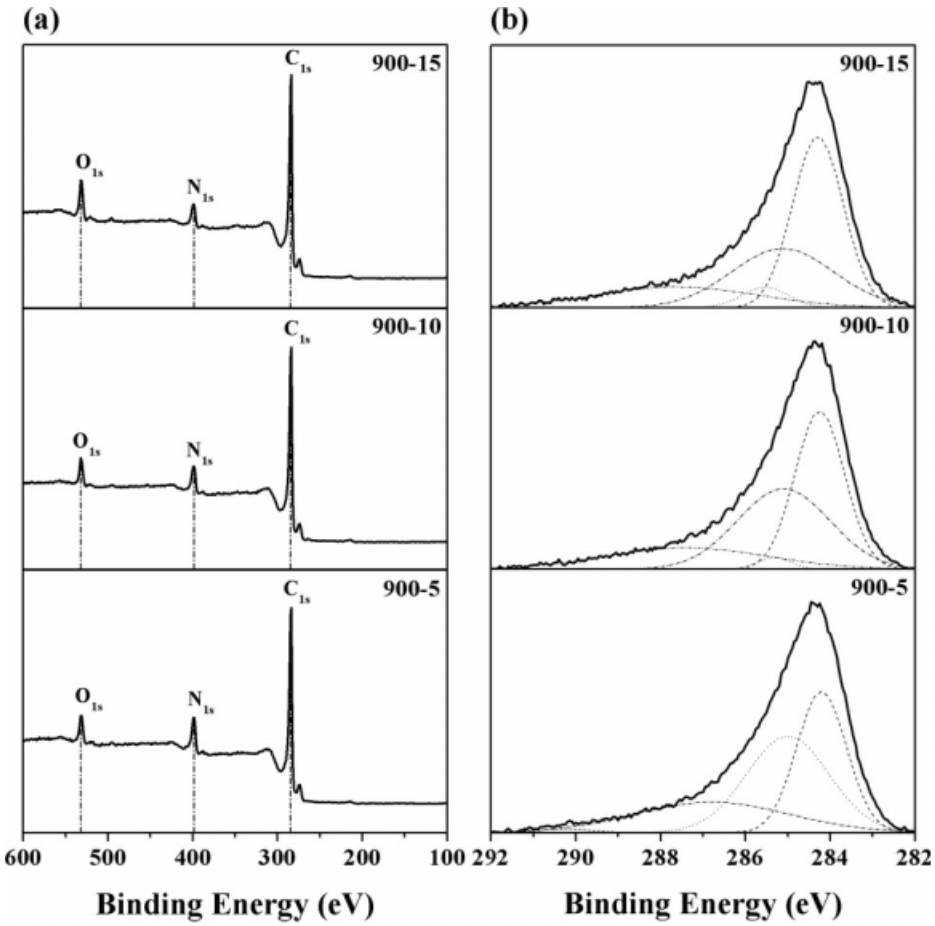

Figure 3 (a) ESCA spectra and (b) Deconvolution spectra of C 1s of ultra-thin ACFs prepared at 900°C with various holding times.

groups.[22,23] The chemical shifts associated with all of the functional groups in ACFs at various activation temperatures and holding times vary (Figs. 3, 4 and Table II), perhaps because of the structural differences among ACFs surfaces. The ESCA spectra of all ACFs have much weaker N 1s and O 1s peaks as than that of C 1s, because of residual nitrogen is present in the fibers. Nitrogen-containing functional groups appear in ACFs at a binding energy of 398.9 eV corresponding to aromatic amines and piperidine structure. As presented in Table II, the ACFs with a higher degree of activation (higher activation temperature, longer holding time) have greater percentages of graphitic carbon, phenolic, and hydroxyl functional groups. The ACFs of lower activation degree exhibits fewer surface functional groups and should have lower surface areas.

The electrochemical capacitance of the ultra-thin activated carbon fibers as electrodes in electrochemical double layers capacitors

Figure 5 presents galvanostatic charge–discharge cycles of ultra-thin ACFs at a current load of 1 mA. In each case, the charge–discharge curves were almost linear indicating that an effective electrode/electrolyte interface was formed in the present experimental cells and that the cells successfully operated as EDLCs. Both curves under these conditions revealed a weak IR drop suggesting that aqueous H_2SO_4 electrolyte had high ionic conductivity and formed good contact with the ACF electrodes. However, the charge curves of the ACFs prepared at 900°C for 5 min are not symmetrical with the discharge curves because the charge profile is raised by the over-potential that is established by the internal resistance, and the discharge profile is lowered for the same reason. The specific capacitances were determined from the discharge curve observed after the IR drop. Table III presents the specific capacitances of the ACF electrodes for various activation temperatures and holding times. Activation at 900°C from 5 to 15 min yielded ACF electrodes with specific capacitances of 74 to 220 F g^{-1}. The specific capacitances of the ACF electrodes that were prepared at 1000°C increased with holding time to 283 F g^{-1} (10 min), then decreased to 231 F g^{-1} (15 min) with further activation. These results agree closely with

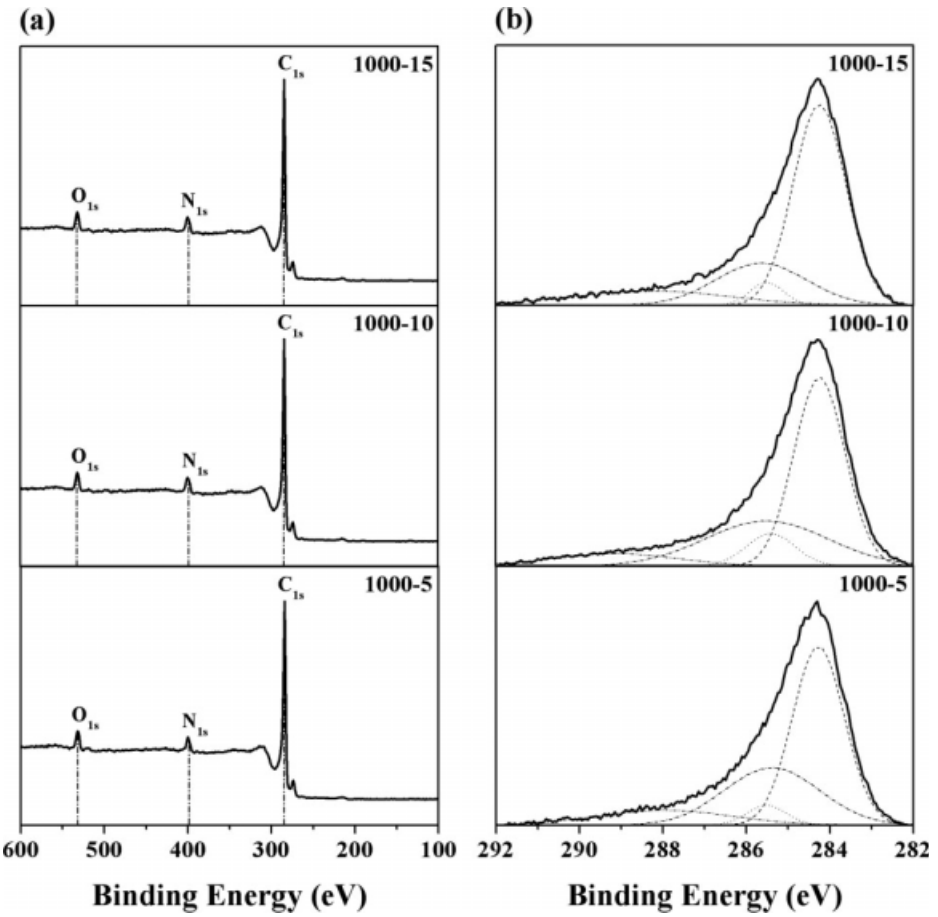

Figure 4 (a) ESCA spectra and (b) Deconvolution spectra of C 1s of ultra-thin ACFs prepared at 1000°C with various holding times.

those from cyclic voltammograms. Figure 6 plots cyclic voltammograms for unit EDLCs with the ACF electrodes using aqueous H_2SO_4 solution were obtained between potentials of 0 and 0.75 V at scanning rates of 6 mV s^{-1}. None of the voltammograms in Figure 6 includes peaks that reveal oxidative–reductive processes in which, indicating that these aqueous H_2SO_4 electrolytes were stable over the range of applied potentials. As the activation temperature and holding time increased, the sharp of cyclic voltammograms tended to become rectangular and similar to those of typical capacitors revealing that charge and discharge occurred reversibly at the electrode/electrolyte interface.

A direct relationship is typically believed to exist between the BET surface area and the double layer capacitance of porous carbons. Theoretically, a higher BET surface area of ACFs is expected to be associated with higher specific capacitances. As the holding time increases upon activation at 900°C, the specific capacitances increased with BET surface area, approaching a maximum of 220 F g^{-1} (1294 m^2 g^{-1}), revealing that a higher BET surface area, more mesopores (Fig. 1), and more oxygen-containing

TABLE II
Relative Percentage of Functional Groups on the ACFs Obtained by ESCA

		Relative atomic percentage of functional groups			
Temperature (°C)	Time (min)	Graphitic carbon	Phenolic (hydroxyl)	Carbonyl	Carboxylic
900	5	60.8	9.7	3.7	3.5
	10	61.9	8.5	6.4	2.1
	15	63.2	8.2	6.6	1.2
1000	5	67.4	13.2	2.3	2.2
	10	70.3	11.8	5.9	1.8
	15	71.7	12.8	4.2	1.6

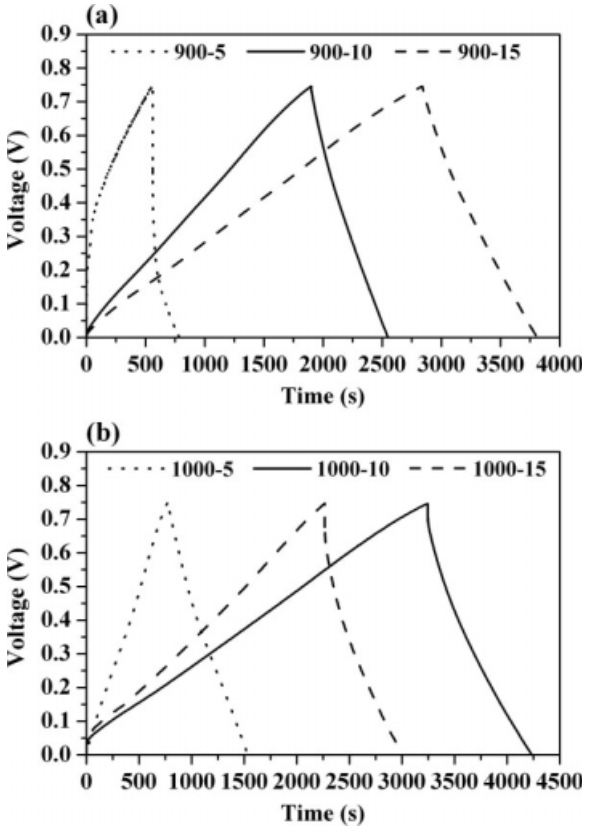

Figure 5 Galvanostatic charge-discharge curves of ultra-thin ACFs prepared at (a) 900°C and (b) 1000°C with a constant loading current of 1 mA.

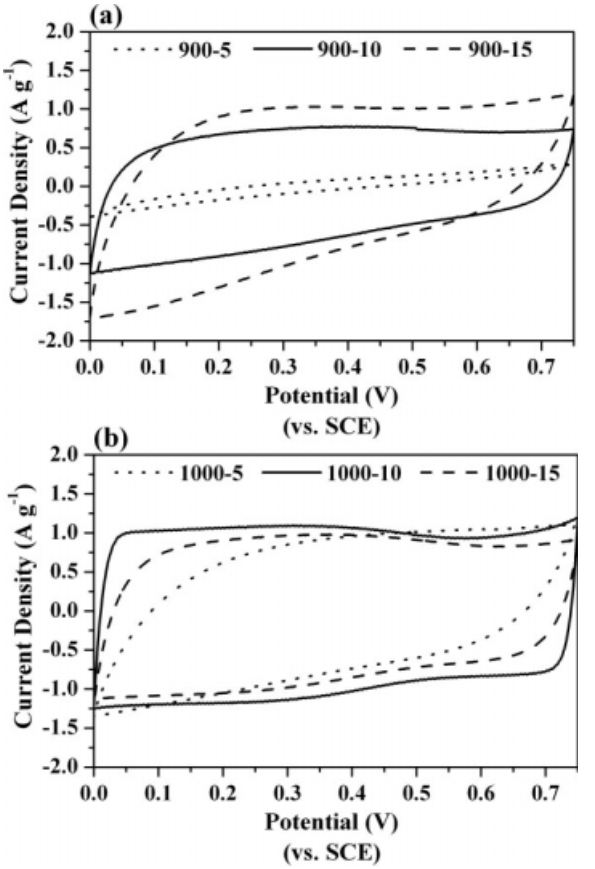

Figure 6 Cyclic voltammetry curves of ultra-thin ACFs prepared at (a) 900°C and (b) 1000°C with scan rate of 6 mV s^{-1}.

functional groups (Table II) promote the specific capacitances of EDLCs. However, the specific capacitance is more complex upon activation at 1000°C. The specific capacitance initially increased with holding time up to 10 min, reaching a maximal value of 283 F g^{-1} (1408 m^2 g^{-1}), and then declined to 231 F g^{-1} (1081 m^2 g^{-1}). The decrease in specific capacitance was associated primarily with a severe reaction that reduced porosity, surface areas, and the number of functional groups in the resultant ACFs. These results reveal that although the BET surface area is a very important parameter, the EDLCs also seem to depend on other characteristics of the ACFs probably the pore size distribution and the surface chemistry.

TABLE III
Capacitances of Ultra-Thin ACF Electrodes

Activation temperature (°C)	Holding time (min)	Capacitance (F g^{-1})
900	5	74
	10	167
	15	220
1000	5	139
	10	283
	15	231

CONCLUSIONS

The electrochemically accessible surface area dominates the specific capacitances of electrochemical double layer capacitor (EDLC) cells with ultra-thin ACF electrodes by the double-layer charge/discharge mechanism. In this investigation, ACFs with high capacitance were prepared using steam activation. The results obtained for ACFs at various activation temperatures and holding times reveal that specific capacitances increase with surface area, to a maximum of 283 F g^{-1} at a surface area of 1408 m^2 g^{-1} (activated at 1000°C for 10 min).

No linear relationship was observed for the ACFs, implying that apart from factors other than the BET surface area, such as the structure, number of surface functional groups and pore size distribution also contribute significantly to the capacitance of the ACFs. Capacitance is observed to increase with the volumes of micropores and mesoporepores. The surface chemistry of the ACFs with the most oxygen-contain functional groups, and the highest capacitance (283 F g^{-1}), was clearly observed. Based on the results herein, the ultra-thin ACFs are expected to

contribute substantially to EDLC devices with excellent electrochemical performance.

References

1. Caturla, F.; Molina-Sabio, M.; Rodrıǵuez-Reinoso, F. Carbon 1991, 29, 999.
2. Jagtoyen, M.; Thwaites, M.; Stencel, J.; McEnaney, B.; Derbyshire, F. Carbon 1992, 30, 1089.
3. Teng, H.; Yeh, T. S. Ind Eng Chem Res 1998, 37, 58.
4. Lozano-Castello, D.; Lillo-Rodenas, M. A.; Cazorla-Amoros, D.; Linares-Solano, A. Carbon 2001, 39, 741.
5. Shimazaki, K.; Ogawa, H. Nippon Kagaku Kaishi 1992, 7, 745.
6. Otani, S.; Kokubo, Y.; Koitabashi, T. Jpn Bull Chem Soc 1970, 43, 3291.
7. Tang, M. M.; Bacon, R. Carbon 1964, 2, 211.
8. Arons, G. N.; Macnair, R. N. J Text Res 1972, 42, 60.
9. Bonnefoi, L.; Simon, P.; Fauvarque, J. F.; Sarrazin, C.; Sarrau, J. F.; Dugast, A. J Power Sources 1999, 80, 149.
10. Jurewicz, K.; Delpeux, S.; Bertagna, V.; Beguin, F.; Frackowiak, E. Chem Phys Lett 2001, 347, 36.
11. Zheng, J. P.; Cygan, P. J.; Jow, T. R. J Electrochem Soc 1995, 142, 2699.
12. Tuinstra, F.; Koening, J. L. J Chem Phys 1970, 53, 1126.
13. Niu, C.; Sichel, E. K.; Hoch, R.; Moy, D.; Tennent, H. Appl Phys Lett 1997, 70, 1480.
14. Qu, D. J Power Sources 2002, 109, 403.
15. Brunouer, S.; Emmet, P.; Teller, E. J Am Chem Soc 1938, 60, 309.
16. Kruk, M.; Jaroniec, M.; Bereznitski, Y. J Colloid Interface Sci 1996, 182, 282.
17. Ryu, Z.; Zheng, J.; Wang, M. Carbon 1998, 36, 427.
18. Seaton, N. A.; Walton, J. P. R. B.; Quirk, N. Carbon 1989, 27, 853.
19. Oliver, J. P. J Porous Mater 1995, 2, 9.
20. Montes-Moran, M. A.; Young, R. J Carbon 2002, 40, 845.
21. El-Geundi, M. S. Adsorpt Sci Technol 1997, 15, 777.
22. Nakayama, Y.; Soeda, F.; Ishitani, A. Carbon 1990, 28, 21.
23. Proctor, A.; Peter, M. A. Carbon 1983, 21, 53.